ChemPubSoc Europe

DOI: 10.1002/ejic.201800158

EurJIC European Journal of Inorganic Chemistry

Full Paper

Self-Assembly

CLUSTER ISSUE

Self-Assembly of Polyoxometalate–Peptide Hybrids in Solution: Elucidating the Contributions of Multiple Possible Driving Forces

Jiancheng Luo,[a] Baofang Zhang,[a] Carine Yvon,[b] Marie Hutin,[b] Selim Gerislioglu,[c] Chrys Wesdemiotis,[c] Leroy Cronin,*[b] and Tianbo Liu*[a]

Abstract: Incorporating the building blocks of nature (e.g., peptides and DNA) into inorganic polyoxometalate (POM) clusters is a promising approach to improve the compatibilities of POMs in biological fields. To extend their biological applications, it is necessary to understand the importance of different non-covalent interactions during self-organization. A series of Anderson POM–peptide hybrids have been used as a simple model to demonstrate the role of different interactions in POM–peptide (biomolecules) systems. Regardless of peptide chain length, these hybrids follow similar solution behaviors, forming hollow, spherical supramolecular structures in acetonitrile/water mixed solvents. The incorporation of peptide tails introduces interesting stimuli-responsive properties to temperature, hybrid concentration, solvent polarity and ionic strength. Unlike the typical bilayer amphiphilic vesicles, they are found to follow the blackberry-type assemblies of hydrophilic macroions, which are regulated by electrostatic interaction and hydrogen bonding. The formation of electrostatic assemblies before the supramolecular formation is confirmed by ion-mobility mass spectrometry (IMS-MS).

Introduction

Inorganic–organic hybrid molecules represent a good toolbox to explore self-assembly as they combine inorganic (well-defined structures, adjustable electronic properties) with organic (soft materials with good processability) compounds for applications in soft functional materials.[1] Among them, polyoxometalate (POM)-based hybrids are particularly attractive due to their desired properties as catalysts,[2] in photovoltaics,[3] molecular magnetism,[4] and biochemistry.[5] POMs are a large group of metal oxide molecular clusters,[6] and are ideal building blocks to develop novel hybrid materials, along with others such as polyhedral oligomeric silsesquioxane (POSS) and fullerene (C_{60}). Incorporating organic ligands into these inorganic components can improve their compatibility in hydrophobic domains, thus expand their applications.[7] For example, the POM–organometallic hybrids exhibit greater catalytic activity and stability than the related organometallic precursors[8] and the POM–chromophore systems show the quenching of luminescence properties due to the intramolecular electron transfer from the chromophore to the polyoxometalates.[9] The organic linkers also enable the design of complex hybrid molecules involving different clusters, such as POM–POSS, POM–C_{60} and POSS–C_{60} hybrids.[10]

Meanwhile, a considerable number of studies have focused on the amphiphilic properties and the consequent self-assembly of hybrid molecules.[11] The molecular architecture of the hybrids is important for determining the critical driving forces for their self-assembly in solution. For instance, a single Dawson linked with long alkyl tails shows the typical surfactant properties (e.g., form micelles or bilayer vesicles) driven by the hydrophobic interaction.[12] On the other hand, the "triangular" shaped hybrids containing three Dawsons only exhibit the self-assembly of hydrophilic macroions, forming single-layered, vesicle-like, blackberry structures because the electrostatic interaction from the clusters is dominant over the hydrophobic interaction.[13] A more systematic example is the tri-armed POSS-organic hybrids. With the long polystyrene (PS) linker, the hybrid shows the properties of amphiphilic surfactants, while with the same topology but shorter linker, the hybrid behaves like macroions.[14] The tricky case is the "dumb-bell" shaped hybrids. We have reported that they form single-layered vesicular structures in polar solvents by using two Dawsons facing the solvent.[15] Originally the assemblies are considered as surfactant vesicles. But after a more thorough consideration, we think that another possibility cannot be ignored – the assemblies of "dumb-bell" hybrids might be blackberry structures, i.e., the middle linkers may not be able to form a compact hydro-

[a] *Department of Polymer Science, University of Akron*
Akron, OH 44325, USA
E-mail: tliu@uakron.edu
http://gozips.uakron.edu/~tliu/
[b] *WEST Chem, School of Chemistry, University of Glasgow,*
University Avenue, Glasgow, G12 8QQ, UK
E-mail: lee.cronin@glasgow.ac.uk
[c] *Department of Chemistry, University of Akron*
Akron, OH 44325, USA

Supporting information and ORCID(s) from the author(s) for this article are available on the WWW under https://doi.org/10.1002/ejic.201800158.

phobic domain (given the packing parameters of the hybrids). The relative size ("functionality") of the organic linker determines which attractive force (counterion-mediated or hydrophobic) is dominant, then consequently determines the nature of the final supramolecular structures. Incorporating the "functional linkers" onto the POM clusters can make the self-assembly with more stimuli-responsive properties[16] (e.g., temperature, pH, metal ions, solvent polarity, electric fields and light), which show the great interest for drug delivery,[17] catalyst recovery[18] and the design of bio-sensors.[19] Given this plethora of potential applications we think that exploring the fundamentals of self-assembly is important if a greater system level control is to be gained.

Exploring POM hybrids that are decorated with biologically active moieties (e.g. Nucleic acids, peptides, carbohydrates) is important due to their biological activities.[20] In this regard some studies have focused on understanding the interactions between polyoxometalates and biomacromolecules. The high binding activities of polyoxometalates to the biomacromolecules (e.g., proteins) has been reported by several groups,[21] which are mainly attributed to the electrostatic interaction. Also, due to the high binding activities, POMs have been considered as an effective inhibitor to various biological processes, such as DNA binding activities of oncogene Sox2[22] and amyloid β-peptide aggregation.[23] As such further understanding of the interactions in POM-biomacromolecules systems still remain a challenge. This is because of the structural complexity of the POMs and the conformational flexibility of the biomacromolecules, as well as the existence of multi-type interactions. To systematically explore this, covalently grafting biomolecules onto POM clusters is a viable pathway to achieve controllable structures and biological functions with the advantage of improving the compatibility in POM-biomacromolecules systems.

In this paper, we report our study on the self-assembly of a series of peptide-Anderson-peptide hybrids in order to understand the different interactions found in POM-biomolecule systems. These hybrids with the same architectures (tail-POM-tail) show self-assembly behaviors that are modulated by multiple

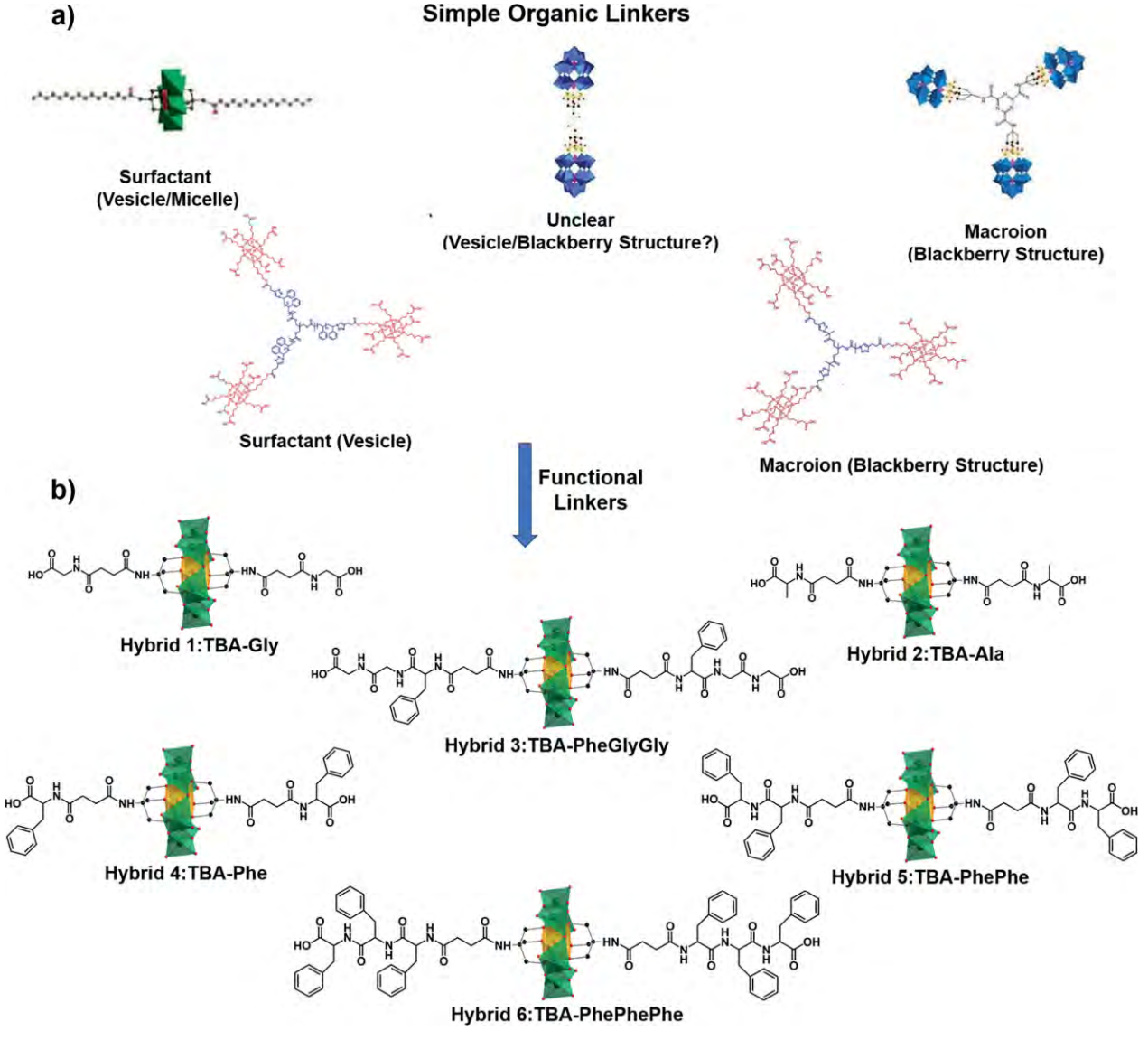

Figure 1. a) Molecular structures of hybrids with simple organic linkers. b) Molecular structures of six POM–peptide hybrid clusters with the functional tails.

external stimuli including temperature, concentration, ionic strength and solvent polarity. The functional peptide tails lead to possible electrostatic interaction (charged chains), hydrophobic interaction, π–π stacking (aromatic rings) as well as hydrogen bonding to Anderson clusters. Since it is difficult to simultaneously study these interactions with isolated molecules, self-assembly provides a straightforward method to explore these interactions. By carefully designing the self-assembly conditions and studying the assembly/disassembly behaviors, the roles of different interactions can be evaluated. This method may provide a guidance for further investigating the interactions in more complex systems.

Results and Discussion

Anderson clusters functionalized with six types of c-terminus peptide chains were chosen for this study, as shown in Figure 1b. Their syntheses have been published recently.[24] For each hybrid, two identical peptide chains were symmetrically grafted onto one Anderson-type cluster, with TBA (tetrabutyl ammonium) being counterions.

Self-Assembly of Anderson POM–Peptide Hybrids in Acetonitrile/Water Mixed Solvents

These hybrids are quite soluble in polar organic solvents such as acetonitrile and dimethylformamide (DMF). However, due to the relatively hydrophobic TBA counterions, they are less soluble in water (the maximum solubility of the TBA-Ala and TBA-Gly is ca. 0.5 mg/mL, while other hybrids such as TBA-Phe are insoluble in water). To prepare the solutions, the hybrids were first dissolved in acetonitrile then water was slowly added to ensure that the solutions remained homogeneous (as confirmed by very low scattered intensity from SLS measurements, <100 kcps; reference intensity for benzene ≈ 40 kcps). Under these conditions, supramolecular structures were observed in the acetonitrile/water mixed solvents with acetonitrile volume contents from 10 % to 80 %. As shown in Figure 2a, these self-assembly processes went through a lag phase of 5–10 days (low scattered intensity), after which the intensity continuously increased until plateauing at a steady state after 15–22 days, indicating the completion of the formation of large self-assembled structures. The scattered intensity did not further increase with time, suggesting that the process was likely a thermodynamically favored self-assembly, instead of a continuous nucleation and aggregation. Nuclear magnetic resonance (NMR) studies, performed on samples more than one month old also showed broad peaks which suggested the self-assembly of hybrids (Figure S1), due to the slower diffusion of the larger structures.

Dynamic light scattering (DLS) data was collected during the entire self-assembly process (e.g., TBA-Phe). From the CONTIN[25] analysis, the hydrodynamic radius (R_h) values of the assemblies at different scattering angles show no angular dependence, which demonstrates the spherical morphology of the assemblies (Figure 2c). Moreover, the radius of gyration (R_g) from the static light scattering (SLS) measurements is very close to the R_h when extrapolating R_h to zero degree of scattering angle (Figure S2), strongly suggesting a hollow, spherical nature for the assemblies. Transmission electron microscopy (TEM) images further confirm these results. From the results, all six hybrids follow similar solution behaviors to form hollow-spherical structures regardless of their chain length.

Identification of the Interactions of POM–Peptide Hybrids via their Self-Assembly Behaviors

It is important to determine the major driving force for the self-assembly among different physical interactions. To achieve this, a series of sample solutions (0.2 mg/mL) with various aceto-

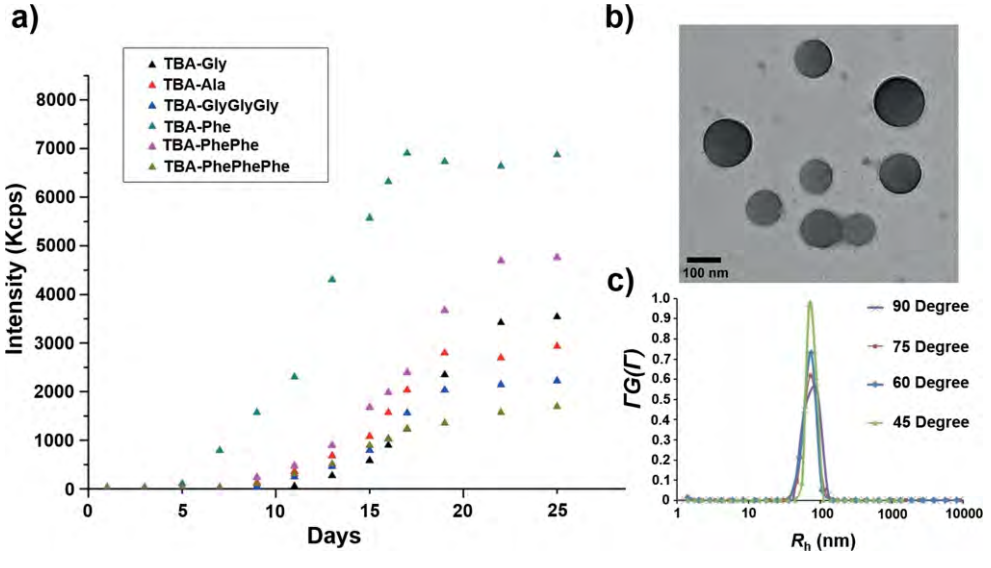

Figure 2. a) Total scattered intensity of six hybrid clusters at 90° angle (0.2 mg/mL, acetonitrile/water = 50:50, v/v) with time. b) TEM images of the spherical structures from 0.2 mg/mL TBA-Phe (acetonitrile/water = 50:50, v/v). The scale bar is 100 nm. c) CONTIN analysis of 0.2 mg/mL TBA-Phe solutions at different angles (acetonitrile/water = 50:50, v/v), $R_{h,0}$ = 70 nm.

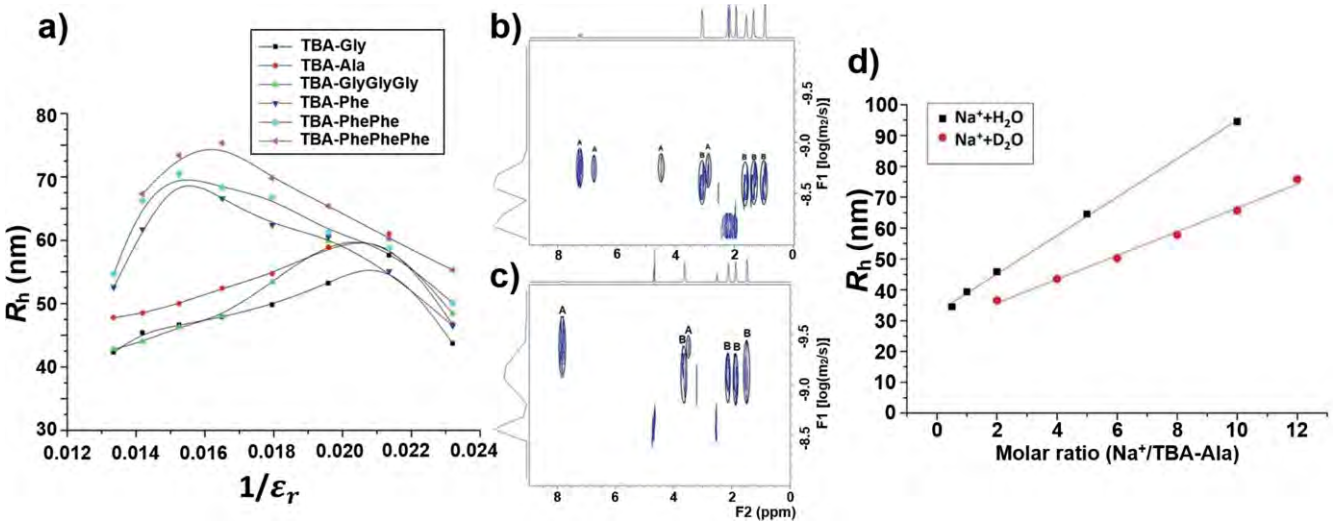

Figure 3. a) Hydrodynamic radius (R_h) change of six hybrids supramolecular structures in various acetonitrile/water mixed solvents. b) 2D DOSY results of TBA-Phe in [D_3]acetonitrile. Signal A comes from the peptide tails and signal B comes from the TBAs. c) 2D DOSY results of TBA-Phe in D_2O/[D_3]acetonitrile mixed solvents. Signal A comes from the peptide tails and signal B comes from the TBAs. d) Hydrodynamic radius (R_h) of TBA-Ala depending on Na^+ concentration in H_2O and D_2O.

nitrile/water volume contents were prepared, to explore the effect of solvent polarity. The solutions were kept at room temperature and R_h values of the assemblies were measured when the solutions reached equilibrium. It has been shown that if the self-assembly process is charge-regulated, the assembly size with the inverse of dielectric constant of the solvents will have a linear relationship.[26] However, in the current system, the size trends of these assemblies seem to be more complicated. As shown in Figure 3a, the R_h values of these assemblies become larger with increasing acetonitrile content (inverse of dielectric constant) at first, while they start to continuously drop when further increasing the acetonitrile content. This indicates that multi-type driving forces are involved in the self-assembly process.

Counterion-mediated attraction should be involved in the self-assembly process. The negative charges may come from two possible sources: the deprotonation of carboxylic acid groups and the dissociation of the TBA counterions. They will be discussed separately. Generally, the deprotonation degree of the carboxylic acid groups can be calculated by measuring the solution pH. However, the pH value measured from acetonitrile/water mixed solvents cannot be directly used unless it is possible to calibrate the relationship between the degree of deprotonation and the polarity of the solvent. Hydrochloric acid solutions in acetonitrile/water mixed solvents (20, 40 and 80 vol. % of water) with different concentrations (from 0.01 mM to 0.1 mM) were used as the control samples (Table S1). The results show that the polar solvents can induce more deprotonation. For instance, the degree of deprotonation of TBA-Phe (0.2 mg/mL) increases from 5 % to 13 %, and further increases to 25 % when the water content increases from 20 % to 40 % and 80 %, respectively. Thus, it can be concluded that the carboxylic acid groups will carry more charge when the solvent polarity is increased. Another factor, the dissociation of the TBA counterions, was studied by the Diffusion-Ordered Spectroscopy (DOSY)[27] NMR spectroscopy. We have observed that polar solvents induce significantly more dissociation of the simple counterions (e.g., Na^+) around $Mo_{72}V_{30}$ macroanions in an earlier study.[28] For bulky TBA counterions, in pure acetonitrile, their diffusion rates are slightly higher than the hybrid clusters from DOSY NMR, indicating that the TBAs are partially released from the clusters (Figure 3b). However, when adding water into acetonitrile, the TBAs diffuse much faster than the clusters, suggesting stronger TBA dissociation at higher water content, making the clusters more negatively charged (Figure 3c).

When the hybrids have a higher net charge at high water content, the assembly sizes should be smaller. Solution behaviors of these hybrids can also provide insight about the role of hydrophobic interaction, which might affect the assembly size. The three hybrids, TBA-Phe, TBA-PhePhe and TBA-PhePhePhe (Figure 1b), have similar assembly sizes in the mixed solvents. For example, their assembly sizes in 50 % acetonitrile are 62 nm, 67 nm and 70 nm, respectively. Their corresponding scattered intensities are ca. 6,800 Kcps, 4,600 Kcps and 1,700 Kcps, respectively. Based on the simplified Rayleigh-Gans–Debye equation for hollow spheres:[29]

$$I \propto C \cdot M_w = C \cdot R_h^2$$

where I is the total scattered intensity from the solution, C and M_w are the concentration and the mass of the assemblies, respectively. According to their similar R_h values and their corresponding scattered intensities, it can be estimated that the order of assemblies' concentration is TBA-Phe > TBA-PhePhe > TBA-PhePhePhe; this order also reflects the tendency to self-assemble in the same mixed solvent. Considering the order of hydrophobicity is TBA-Phe<TBA-PhePhe<TBA-PhePhePhe, it thus can be concluded that the hydrophobic interaction is not the major driving force for the self-assembly. Otherwise the most hydrophobic hybrid, TBA-PhePhePhe, should have the strongest tendency to assemble. Moreover, these hybrids follow the similar size trends regardless of the presence of aromatic rings on the peptide chains, implying that the π–π stacking is also not dominant driving force.

Another possible driving force is hydrogen bonding, which is abundant in bio-systems, such as the formation of β-sheets.[30] Therefore, it is reasonable to speculate that the peptide tails with sufficient sites of hydrogen binding could influence the assembly sizes of hybrids. The contribution of hydrogen bonding can be estimated by studying the temperature effect on the self-assembly. However, since the deprotonation of carboxylic acids is also temperature dependent, this approach is not the best option here. An alternative way is to study the self-assembly behaviors of hybrids in H_2O and D_2O, respectively. D_2O has different strength of hydrogen bonding compared with H_2O, which can impact the assembly of hybrids if hydrogen bonding is dominant. TBA-Ala was used for this study because of its good solubility in H_2O and D_2O. Owing to the strong repulsion among individual hybrid molecule in H_2O and D_2O, no large structures were observed. Additional NaCl was added to trigger the self-assembly. As shown in Figure 3d, the assembly size increased linearly with increasing Na^+ concentrations. Importantly, at low Na^+ concentrations, the difference in R_h values between the assemblies in H_2O and D_2O was quite small, indicating that the hydrogen bonding was not dominant. However, the size discrepancy became larger at higher Na^+ concentrations, showing a sign of enhancing the domination of hydrogen bonding. The Na^+ ions can screen the net charge and reduce the electrostatic repulsion between the hybrid molecules, while the difference in hydrogen bonding between H_2O and D_2O will remain almost identical and become more dominant when the electrostatic repulsion is weaker. This suggests that, even though the hydrogen bonding can affect the assembly process, it is weaker than the electrostatic interaction among the hybrids. Only when the electrostatic repulsion is significantly screened by extra ions will the hydrogen bonding become important.

Therefore, in polar solvents, weak hydrogen bonding and strong electrostatic interactions simultaneously affect the size trends of POM-peptide hybrids. At higher water content, the electrostatic interaction is dominant, which leads to the charge-regulated mechanism (linear increase of assembly size with increasing acetonitrile content). At lower water content, the electrostatic interaction decreases dramatically; the assembly size decreases with increasing acetonitrile content due to the gradual domination of hydrogen bonding. The hydrophobic interaction and π–π stacking have no obvious effects on the self-assembly process.

Identification of the Self-Assembly Mechanism

For POM-based hybrids containing two long alkyl chains, the self-assembly is driven by hydrophobic interaction, forming bilayer vesicles in polar mixed solvents – similar to amphiphilic surfactants.[11a] However, some of current hybrids (e.g., TBA-Ala and TBA-Gly) contain very hydrophilic, charged tails which do not contribute to any hydrophobic interactions. Moreover, according to the conclusion above, the current assemblies are controlled by electrostatic interaction and hydrogen bonding rather than the hydrophobic interaction. Therefore, instead of forming bilayer vesicles, we speculate that they follow the self-assembly of hydrophilic macroions to form single-layered blackberry-type structures. To confirm this, further studies were conducted to reveal the function of peptide tails in regulating the self-assembly. The R_h values of the assemblies show an unexpected dependence on both temperature and hybrid concentration. For example, the R_h values of TBA-Phe gradually changes from 40 nm to 72 nm when increasing hybrid concentration from 0.02 mg/mL to 0.2 mg/mL (Figure 4b). Also, the

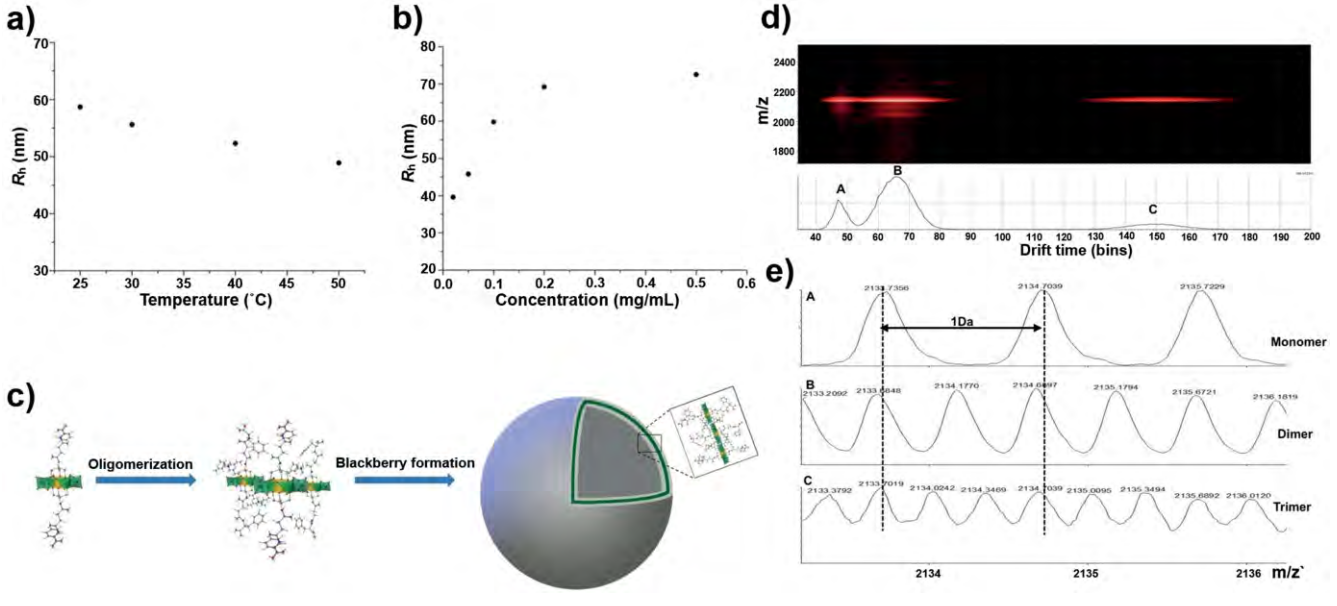

Figure 4. a) Hydrodynamic radius (R_h) change of formed TBA-Phe supramolecular structures depending on temperature. b) Hydrodynamic radius (R_h) change of formed TBA-Phe supramolecular structures depending on hybrid concentration. c) Illustration of single-layer blackberry-like formation process. The TBAs are strongly associated with Anderson POMs, resulting into far distance between the protons in TBAs and the peptide tails. d) IMS-MS results of TBA-Phe during self-assembly, three major peaks are observed along drift time. e) Individual isotope pattern of three peaks around 2134 *m/z*.

disassembly process can be further controlled by either increasing the hybrid concentration (> 2 mg/mL) or decreasing the temperature (< 20 °C). These self-assembly behaviors reveal the role of the charged chains, which can be correlated to the degree of deprotonation of the carboxylic acids. In previous studies, supramolecular self-assembly of POM-based hybrids are observed only when the solubility of tails is much less than the Anderson clusters (Table S2), where the tails bend significantly induced by hydrophobic interaction. However, since the peptide tails are quite soluble in acetonitrile/water mixed solvents, rather than overcoming the high bending energy, the tails prefer to face out in solution. 2D Nuclear Overhauser Effect Spectroscopy (NOESY) NMR studies reveal a long distance (> 5 Å) between the protons of the TBAs and the peptide tails (Figure S3), suggesting that the TBAs are very free in solution. This is different from the bilayer vesicle structures formed by Lindqvist–pyrene hybrids.[16a] The latter involves strong association between the TBAs and the organic tails to fill the hydrophobic layers of the vesicles.

Oligomer Formation During the Self-Assembly Process

The blackberry structure formation is usually slow owing to a high activation energy barrier (e.g., ~115 kJ/mol for $Mo_{72}Fe_{30}$).[31] This process includes a slow process from monomers to oligomers and a fast process from oligomers to blackberry structures. Herein, the Ion-Mobility Mass Spectrometry (IMS-MS) experiments provide important molecular-level insight on the oligomer stage of the self-assembly. Mass spectrum of the sample showed a molecular ion peak at 2134 *m/z* (Figure S4). During the ionization, formation of multiple charged ions of different oligomers resulted in the overlap of isotope patterns of the monomers and oligomers at the same *m/z* value (2134 *m/z*). From the IMS-MS analysis, the monomers and oligomers were successfully separated along the drift time scale (Figure 4d). Three types of major oligomer structures were identified: 1^- (monomers each losing one TBA^+), 2^- (dimers losing one TBA^+ and one H^+), and 3^- (trimers each losing one TBA^+ and two H^+). From relative abundance of each peak, it also can be concluded that the dimers are dominant, which agrees well with the previous analytical sedimentation study.[31]

Conclusions

In summary, six Anderson-peptide hybrids with different chain lengths and architectures were studied in order to evaluate the contributions to their self-assembly behaviors. The strong electrostatic interaction and weak hydrogen bonding simultaneously control the self-assembly process, whereas the hydrophobic interaction and π–π stacking have no obvious effect. These hybrids all form single-layered blackberry-type assemblies in polar organic solvents. The IMS-MS results confirm the oligomer stage during the slow blackberry structure formation. These hybrids exhibit multi-stimuli responsive self-assembly behaviors to temperature, hybrid concentration, solvent polarity and ionic strength.

Experimental Section

IMS-MS Experiments: ESI-IMS-MS experiments were carried out with Waters Synapt G1 HDMS quadrupole/time-of-flight (Q/TOF) mass spectrometer (Waters, Milford, MA), equipped with traveling wave ion mobility chamber. Samples having 5 μg/mL concentration injected to the instrument with a flow rate of 20 μL/min. Instrument parameters were adjusted as follows: ESI capillary voltage, 3.16 kV; sample cone voltage, 35 V; extraction cone voltage, 3.2 V; desolvation gas flow, 500 L/h (N_2); trap collision energy (CE), 6.0 eV; transfer CE, 4.0 eV; trap gas flow, 1.5 mL/min (Ar); IM gas flow, 22.7 mL/min (N_2); source temperature, 50 °C; desolvation temperature, 150 °C; IM traveling wave velocity, 200 m/s; and IM traveling wave height, 10.0 V. All the mass spectra were obtained at negative mode. Therefore, the observed ions were formed by either loss of a counterion, $[M - TBA]^-$, loss of a H possibly from the carboxylic acid ends, $[M - H]^-$, or even both, $[M - TBA - H]^{2-}$. Ions having different charge states were observed depending on the number of TBA or H losses.

Laser Light Scattering: Both dynamic light scattering (DLS) and static light scatting (SLS) data were measured on a Brookhaven Instruments Inc. light scattering spectrometer, equipped with a diode-pumped solid-state (DPSS) laser operating at 532 nm and a BI-9000AT multichannel digital correlator. The SLS was performed over a broad range of scattered angles from 30° to 90°, with a 2° interval. The radius of gyration (R_g) was calculated using a partial Zimm plot derived from the Rayleigh-Gans–Debye equation. The partial Zimm plot stemmed from the following approximate formula: $1/I = C(1+R_g^2\ q^2/3)$. The R_g was determined from the slope and intercept of a plot of $1/I$ vs. q^2. For DLS measurements, the intensity-intensity time correlation functions were analyzed by the constrained regularized (CONTIN) method. The average apparent translational diffusion coefficient, D_{app}, was determined from the normalized distribution function of the characteristic line width, Γ(G). The hydrodynamic radius (R_h) was converted from D through the Stokes–Einstein equation: $R_h = KT/6\pi\eta D$, where k is the Boltzmann constant and η is the viscosity of the solvent at temperature T.

Transmission Electron Microscopy (TEM) Experiments: The TEM images were taken on a JEOL JEM-1230 electron microscope operated at 120 kV. Samples for the TEM analysis were prepared by dropping a small volume of the solution onto a carbon film on a copper grid and drying for several days.

Nuclear Magnetic Resonance Spectroscopy (NMR): All 1D ^1H NMR measurements in the liquid state were measured by a Varian NMRS 500 spectrometer equipped with a 5 mm dual broadband probe. 2D nuclear Overhauser enhancement spectroscopy (2D NOESY) experiments were performed on Varian INOVA 750 with 256 t_1 increments and 16 scans. The relaxation delay varied from 1 to 2 s, and the mixing time changed from 0.2 to 0.6 s. Baseline correction and noise reduction were performed when appropriate. 2D Diffusion Ordered Spectroscopy (2D DOSY) experiments were performed on Bruker 500 MHz spectrometer with the magnetic field gradient g varying from 0 to 32 G/cm in 16–32 steps. All spectra were taken at room temperature. The raw data was fit by CONTIN methods.

Acknowledgments

T. L. acknowledges support from the National Science Foundation (NSF) (CHE1607138) and the University of Akron. L. C. acknowledges support from the EPSRC (EP/J015156/1, EP/L023652/1) and the ERC (project 670467 SMART-POM).

We thank Dr. Zhaoxiong Norm Zheng for help with the DOSY experiments.

Keywords: Hybrids · Non-covalent interaction · Peptides · Polyoxometalates · Self-assembly

[1] a) A. Wight, M. Davis, *Chem. Rev.* **2002**, *102*, 3589–3614; b) C. Sanchez, B. Lebeau, F. Chaput, J. P. Boilot, *Adv. Mater.* **2003**, *15*, 1969–1994; c) S. Günes, H. Neugebauer, N. S. Sariciftci, *Chem. Rev.* **2007**, *107*, 1324–1338; d) C. Sanchez, P. Belleville, M. Popall, L. Nicole, *Chem. Soc. Rev.* **2011**, *40*, 696–753.

[2] a) Y. V. Geletii, B. Botar, P. Kögerler, D. A. Hillesheim, D. G. Musaev, C. L. Hill, *Angew. Chem. Int. Ed.* **2008**, *47*, 3896–3899; *Angew. Chem.* **2008**, *120*, 3960–3963; b) H. Lv, Y. V. Geletii, C. Zhao, J. W. Vickers, G. Zhu, Z. Luo, J. Song, T. Lian, D. G. Musaev, C. L. Hill, *Chem. Soc. Rev.* **2012**, *41*, 7572–7589; c) R. Al-Oweini, A. Sartorel, B. S. Bassil, M. Natali, S. Berardi, F. Scandola, U. Kortz, M. Bonchio, *Angew. Chem. Int. Ed.* **2014**, *53*, 11182–11185; *Angew. Chem.* **2014**, *126*, 11364.

[3] a) L. Xu, M. Lu, B. Xu, Y. Wei, Z. Peng, D. R. Powell, *Angew. Chem. Int. Ed.* **2002**, *41*, 4129–4132; *Angew. Chem.* **2002**, *114*, 4303; b) Y. Yang, L. Xu, F. Li, X. Du, Z. Sun, *J. Mater. Chem.* **2010**, *20*, 10835–10840.

[4] a) J. D. Compain, P. Mialane, A. Dolbecq, I. M. Mbomekallé, J. Marrot, F. Sécheresse, E. Rivière, G. Rogez, W. Wernsdorfer, *Angew. Chem. Int. Ed.* **2009**, *48*, 3077–3081; *Angew. Chem.* **2009**, *121*, 3123–3127; b) J. M. Clemente-Juan, E. Coronado, A. Gaita-Ariño, *Chem. Soc. Rev.* **2012**, *41*, 7464–7478.

[5] a) J. T. Rhule, C. L. Hill, D. A. Judd, R. F. Schinazi, *Chem. Rev.* **1998**, *98*, 327–358; b) A. Seko, T. Yamase, K. Yamashita, *J. Inorg. Biochem.* **2009**, *103*, 1061–1066; c) J. Geng, M. Li, J. Ren, E. Wang, X. Qu, *Angew. Chem. Int. Ed.* **2011**, *50*, 4184-4188; *Angew. Chem.* **2011**, *123*, 4270–4274.

[6] D.-L. Long, E. Burkholder, L. Cronin, *Chem. Soc. Rev.* **2007**, *36*, 105–121.

[7] a) A. Dolbecq, E. Dumas, C. R. Mayer, P. Mialane, *Chem. Rev.* **2010**, *110*, 6009–6048; b) A. Proust, B. Matt, R. Villanneau, G. Guillemot, P. Gouzerh, G. Izzet, *Chem. Soc. Rev.* **2012**, *41*, 7605–7622; c) Y.-F. Song, R. Tsunashima, *Chem. Soc. Rev.* **2012**, *41*, 7384–7402.

[8] a) I. Bar-Nahum, H. Cohen, R. Neumann, *Inorg. Chem.* **2003**, *42*, 3677–3684; b) S. Berardi, M. Carraro, M. Iglesias, A. Sartorel, G. Scorrano, M. Albrecht, M. Bonchio, *Chem. Eur. J.* **2010**, *16*, 10662–10666.

[9] a) B. Matt, S. Renaudineau, L.-M. Chamoreau, C. Afonso, G. Izzet, A. Proust, *J. Org. Chem.* **2011**, *76*, 3107–3112; b) B. Matt, C. Coudret, C. Viala, D. Jouvenot, F. Loiseau, G. Izzet, A. Proust, *Inorg. Chem.* **2011**, *50*, 7761–7768.

[10] a) M.-B. Hu, Z.-Y. Hou, W.-Q. Hao, Y. Xiao, W. Yu, C. Ma, L.-J. Ren, P. Zheng, W. Wang, *Langmuir* **2013**, *29*, 5714–5722; b) H. Liu, C.-H. Hsu, Z. Lin, W. Shan, J. Wang, J. Jiang, M. Huang, B. Lotz, X. Yu, W.-B. Zhang, *J. Am. Chem. Soc.* **2014**, *136*, 10691–10699; c) H. Liu, J. Luo, W. Shan, D. Guo, J. Wang, C.-H. Hsu, M. Huang, W. Zhang, B. Lotz, W.-B. Zhang, *Acs Nano* **2016**, *10*, 6585–6596; d) X.-S. Hou, G.-L. Zhu, L.-J. Ren, Z. Huang, R.-B. Zhang, G. Ungar, L.-T. Yan, W. Wang, *J. Am. Chem. Soc.* **2018**, *140*, 1805–1811.

[11] a) J. Zhang, Y.-F. Song, L. Cronin, T. Liu, *J. Am. Chem. Soc.* **2008**, *130*, 14408–14409; b) M. H. Rosnes, C. Musumeci, C. P. Pradeep, J. S. Mathieson, D.-L. Long, Y.-F. Song, B. Pignataro, R. Cogdell, L. Cronin, *J. Am. Chem. Soc.* **2010**, *132*, 15490–15492; c) S. Landsmann, C. Lizandara-Pueyo, S. Polarz, *J. Am. Chem. Soc.* **2010**, *132*, 5315–5321; d) P. Yin, D. Li, T. Liu, *Chem. Soc. Rev.* **2012**, *41*, 7368–7383.

[12] P. Yin, C. P. Pradeep, B. Zhang, F. Y. Li, C. Lydon, M. H. Rosnes, D. Li, E. Bitterlich, L. Xu, L. Cronin, *Chem. Eur. J.* **2012**, *18*, 8157–8162.

[13] B. Zhang, C. P. Pradeep, L. Cronin, T. Liu, *Chem. Commun.* **2015**, *51*, 8630–8633.

[14] W. Zhang, Y. Chu, G. Mu, S. A. Eghtesadi, Y. Liu, Z. Zhou, X. Lu, M. A. Kashfipour, R. S. Lillard, K. Yue, *Macromolecules* **2017**, *50*, 5042–5050.

[15] a) C. P. Pradeep, M. F. Misdrahi, F. Y. Li, J. Zhang, L. Xu, D. L. Long, T. Liu, L. Cronin, *Angew. Chem. Int. Ed.* **2009**, *48*, 8309–8313; *Angew. Chem.* **2009**, *121*, 8459; b) M. F. Misdrahi, M. Wang, C. P. Pradeep, F.-Y. Li, C. Lydon, L. Xu, L. Cronin, T. Liu, *Langmuir* **2011**, *27*, 9193–9202.

[16] a) D. Li, J. Song, P. Yin, S. Simotwo, A. J. Bassler, Y. Aung, J. E. Roberts, K. I. Hardcastle, C. L. Hill, T. Liu, *J. Am. Chem. Soc.* **2011**, *133*, 14010–14016; b) P. Yin, T. Li, R. S. Forgan, C. Lydon, X. Zuo, Z. N. Zheng, B. Lee, D. Long, L. Cronin, T. Liu, *J. Am. Chem. Soc.* **2013**, *135*, 13425–13432; c) J. Zhou, P. Yin, X. Chen, L. Hu, T. Liu, *Chem. Commun.* **2015**, *51*, 15982–15985; d) F. Haso, J. Luo, B. S. Bassil, B. Artetxe, J. Zhou, P. Yin, S. Reinoso, J. M. Gutiérrez-Zorrilla, U. Kortz, T. Liu, *ChemistrySelect* **2016**, *1*, 4345–4349; e) J. Luo, K. Chen, P. Yin, T. Li, G. Wan, J. Zhang, S. Ye, X. Bi, Y. Pang, Y. Wei, T. Liu, *Angew. Chem. Int. Ed.* **2018**, *57*, 4067–4072; *Angew. Chem.* **2018**, *130*, 4131–4136.

[17] A. P. Griset, J. Walpole, R. Liu, A. Gaffey, Y. L. Colson, M. W. Grinstaff, *J. Am. Chem. Soc.* **2009**, *131*, 2469–2471.

[18] Y. Yang, B. Zhang, Y. Wang, L. Yue, W. Li, L. Wu, *J. Am. Chem. Soc.* **2013**, *135*, 14500–14503.

[19] J. Hu, S. Liu, *Macromolecules* **2010**, *43*, 8315–8330.

[20] a) T. Yamase, *J. Mater. Chem.* **2005**, *15*, 4773–4782; b) C. E. Müller, J. Iqbal, Y. Baqi, H. Zimmermann, A. Röllich, H. Stephan, *Bioorg. Med. Chem. Lett.* **2006**, *16*, 5943–5947.

[21] a) G. Zhang, B. Keita, C. T. Craescu, S. Miron, P. de Oliveira, L. Nadjo, *J. Phys. Chem. B* **2007**, *111*, 11253–11259; b) L. Zheng, Y. Ma, G. Zhang, J. Yao, B. S. Bassil, U. Kortz, B. Keita, P. de Oliveira, L. Nadjo, C. T. Craescu, *Eur. J. Inorg. Chem.* **2009**, *2009*, 5189–5193; c) L. Zheng, Z. Gu, Y. Ma, G. Zhang, J. Yao, B. Keita, L. Nadjo, *J. Biol. Inorg. Chem.* **2010**, *15*, 1079–1085.

[22] K. Narasimhan, S. Pillay, N. R. Bin Ahmad, Z. Bikadi, E. Hazai, L. Yan, P. R. Kolatkar, K. Pervushin, R. Jauch, *ACS Chem. Biol.* **2011**, *6*, 573–581.

[23] M. Li, C. Xu, L. Wu, J. Ren, E. Wang, X. Qu, *Small* **2013**, *9*, 3455–3461.

[24] C. Yvon, A. J. Surman, M. Hutin, J. Alex, B. O. Smith, D. L. Long, L. Cronin, *Angew. Chem. Int. Ed.* **2014**, *53*, 3336–3341; *Angew. Chem.* **2014**, *126*, 3404.

[25] S. W. Provencher, *Comput. Phys. Commun.* **1982**, *27*, 229–242.

[26] M. L. Kistler, A. Bhatt, G. Liu, D. Casa, T. Liu, *J. Am. Chem. Soc.* **2007**, *129*, 6453–6460.

[27] L. Van Lokeren, E. Cartuyvels, G. Absillis, R. Willem, T. N. Parac-Vogt, *Chem. Commun.* **2008**, 2774–2776.

[28] J. M. Pigga, M. L. Kistler, C. Y. Shew, M. R. Antonio, T. Liu, *Angew. Chem. Int. Ed.* **2009**, *48*, 6538–6542; *Angew. Chem.* **2009**, *121*, 6660.

[29] P. Hiemenz, R. Rajagopalan. *Principles of Colloid and Surface Chemistry*, Marcel Dekker, New York, **1997**.

[30] R. Nelson, M. R. Sawaya, M. Balbirnie, A. Ø. Madsen, C. Riekel, R. Grothe, D. Eisenberg, *Nature* **2005**, *435*, 773–778.

[31] J. Zhang, D. Li, G. Liu, K. J. Glover, T. Liu, *J. Am. Chem. Soc.* **2009**, *131*, 15152–15159.

Received: February 1, 2018